Structure
Article

Quantitative Structural Analysis of Importin-β Flexibility: Paradigm for Solenoid Protein Structures

Jade K. Forwood,[1,2,*] Allison Lange,[3] Ulrich Zachariae,[4] Mary Marfori,[2] Callie Preast,[3] Helmut Grubmüller,[4] Murray Stewart,[5] Anita H. Corbett,[3] and Bostjan Kobe[2,*]
[1]School of Biomedical Sciences, Charles Sturt University, Wagga Wagga, New South Wales 2650, Australia
[2]School of Chemistry and Molecular Biosciences Institute for Molecular Bioscience and Centre for Infectious Disease Research, University of Queensland, Brisbane, Queensland 4072, Australia
[3]Department of Biochemistry, Emory University School of Medicine, Atlanta, GA 30322, USA
[4]Max-Planck Institute for Biophysical Chemistry, Am Fassberg 11, 37077 Göttingen, Germany
[5]MRC Laboratory of Molecular Biology, Hills Road, Cambridge CB2 2QH, UK
*Correspondence: jforwood@csu.edu.au (J.K.F.), b.kobe@uq.edu.au (B.K.)
DOI 10.1016/j.str.2010.06.015

SUMMARY

The structure of solenoid proteins facilitates a higher degree of flexibility than most folded proteins. In importin-β, a nuclear import factor built from 19 tandem HEAT repeats, flexibility plays a crucial role in allowing interactions with a range of different partners. We present a comprehensive analysis of importin-β flexibility based on a number of different approaches. We determined the crystal structure of unliganded *Saccharomyces cerevisiae* importin-β (Kap95) to allow a quantitative comparison with importin-β bound to different partners. Complementary mutagenesis, small angle X-ray scattering and molecular dynamics studies suggest that the protein samples several conformations in solution. The analyses suggest the flexibility of the solenoid is generated by cumulative small movements along its length. Importin-β illustrates how solenoid proteins can orchestrate protein interactions in many cellular pathways.

INTRODUCTION

Solenoid proteins, constructed from tandem structural repeats arranged in superhelical fashion, feature in many cellular processes (Kobe and Kajava, 2000). One such process is nucleocytoplasmic transport, in which solenoid proteins constructed from HEAT repeats (the β-karyopherin superfamily) and armadillo (importin-α; Impα) repeats (Kobe et al., 1999; Peifer et al., 1994) constitute the principal transport receptors. A key structural property that differentiates solenoid proteins from other structured proteins is the lack of contacts between distal regions of protein sequence (sequence-distal contacts). For this reason, solenoid proteins are often more flexible than other structured proteins, and this flexibility is an important feature of their specific functions. In terms of flexibility, solenoid proteins are emerging as a structural class that falls between typical globular structured proteins and intrinsically unstructured proteins (Wright and Dyson, 1999).

Importin-β (karyopherin-β1; here abbreviated as Impβ) is the most intensively studied member of the β-karyopherin superfamily. Its sequence consists of 19 tandem HEAT repeats, each repeat a structural unit comprised of two antiparallel (A- and B-) α helices (Andrade and Bork, 1995; Cingolani et al., 1999; Groves et al., 1999; Kobe et al., 1999). The units arrange into a solenoid, with the helices perpendicular to the solenoid axis (A helices on the concave face and B helices on the convex face). Impβ facilitates transport through the nuclear pore complex by transient interactions with FG-nucleoporins that line the central transport channel of the pore (Stewart, 2007). Impβ can carry into the nucleus a range of cargo proteins, which either bind to Impβ directly or through adaptor proteins such as Impα and snurportin1. The Impα/β-mediated nuclear import is considered the most widely used pathway (Lange et al., 2007). Cargo proteins bind to Impα through the classical basic nuclear localization sequence (cNLS); Impα in turn binds to Impβ through its Impβ-binding (IBB) domain, and the trimeric complex enters the nucleus. In the nucleus, the complex is dissociated by binding of RanGTP to Impβ. The direction of the transport is determined by the nucleotide state of Ran (nucleus: RanGTP; cytoplasm: RanGDP), which is in turn established by localizing RanGAP (GTPase-activating protein) and RanGEF (guanine nucleotide exchange factor, RCC1) to the cytoplasm and the nucleus, respectively (Lange et al., 2007; Stewart, 2007).

The structure of Impβ has been studied extensively, using full-length and fragments of human (hImpβ), mouse (mImpβ) and *S. cerevisiae* (Kap95; here abbreviated as yImpβ) proteins bound to different partners (Suel et al., 2006), such as Ran (Forwood et al., 2008; Lee et al., 2005; Vetter et al., 1999), nucleoporins (Bayliss et al., 2000; Liu and Stewart, 2005), and cargo proteins (Cingolani et al., 1999, 2002; Lee et al., 2003; Mitrousis et al., 2008; Wohlwend et al., 2007). Comparison of structures of Impβ bound to these different proteins shows large conformational differences (Cingolani et al., 2000; Conti et al., 2006; Bhardwaj and Cingolani, 2010). The solenoid structure plays a central role through providing a large surface area

that can adjust to different binding partners. The use of different conformational states for different binding functions may finely tune the energies of binding events and ensure the appropriate gradation of affinities in different stages of the pathway (Cansizoglu and Chook, 2007; Conti et al., 2006; Forwood et al., 2008; Fukuhara et al., 2004; Zachariae and Grubmuller, 2008). We present a comprehensive analysis of importin-β flexibility based on a number of different approaches. As the structure of unliganded full-length Impβ has previously only been studied by small-angle X-ray scattering (SAXS) (Fukuhara et al., 2004), we determined the crystal structure of unliganded yImpβ to allow a quantitative comparison with importin-β bound to different partners. We used a number of complementary approaches including molecular dynamics (MD), SAXS, quantitative geometric analyses and TLS (translation/libration/screw) analyses to compare the conformations of the different Impβ structures and analyze the molecular basis of the molecule's flexibility. We conclude that Impβ samples several conformations in solution, which result from cumulative small structural changes along the length of the solenoid. Such flexibility may be important to store internal energy in the structure to control the binding of different partners along the nuclear transport pathway.

RESULTS AND DISCUSSION

Conformational Behavior of Unliganded *S. cerevisiae* Importin-β

Crystal Structure of Unliganded S. cerevisiae *Importin-β*

To enable a complete comparison to be made between different conformations of yImpβ, it was necessary to obtain a crystal structure of the unliganded molecule so that the effects of the binding of different partners could be assessed. We therefore crystallized and determined a 2.4 Å resolution crystal structure of yImpβ. The refined model (R = 18.6%, R_{free} = 22.4%) (Table 1) includes all 861 residues of yImpβ and 168 water molecules. In this structure, the 19 HEAT repeats of yImpβ are arranged in a tightly coiled, compact conformation resembling the shape of a heart (Figure 1). The structure, including the crystal packing, resembles yImpβ in the yImpβ:Nup1 complex (Liu and Stewart, 2005) (rmsd 2.22 Å for 835 Cα atoms). Residues 142–861 (corresponding to HEAT repeats H4-19) superimpose particularly well, while HEAT repeats H1-3 diverge (Figure 1B). The similarity of these two structures suggests that Nup1 binding does not significantly alter the structure of Impβ. The unliganded yImpβ structure also resembles an unliganded mImpβ fragment (residues 1–454) closely (rmsd of 2.7 Å for 418 Cα atoms) (Lee et al., 2000; Figure 1C). The compact conformation appears to be mediated primarily through sequence-distal contacts involving HEAT repeats H2 and H4 interacting with H17 (the principal interactions involve Ser74 in Asp167 in H2/4 and Arg696, Glu737, Asn738 and Gly739 in H17; Table 2). These interactions bury 306 $Å^2$ of surface area, which is smaller than is normally seen in protein:protein interfaces and indicates that the amount of energy required to distort the flexible Impβ solenoid is relatively small. There are also interactions of H8 with H11 and H12, but similar interactions are found in other yImpβ structures (Forwood et al., 2008; Lee et al., 2005; Liu and Stewart, 2005) and so these are unlikely to contribute to the specific conformation of the unliganded state observed here.

Table 1. Structure Determination

Diffraction Data Statistics	
Space group	$P2_1$
Unit cell dimensions	
a, b, c (Å)	58.17, 127.25, 68.52
β (°)	102.23
Resolution (Å)	30–2.4 (2.49–2.40)[a]
Observations	251,525 (24,460)
Unique reflections	37,902 (3727)
Completeness (%)	97.1 (95.5)
Multiplicity	6.6 (6.6)
Rmerge[b] (%)	7.5 (52.9)
$<I/\sigma(I)>$	11.4 (2.6)
Refinement Statistics	
Resolution (Å)	30–2.4 (2.46–2.40)
Number of unique reflections	37,873 (2648)
R_{cryst}[c] (%)	20.5
R_{free}[d] (%)	23.5
Number of Nonhydrogen Atoms	
Protein	6654
Solvent	83
Mean B-factor ($Å^2$)	67.6
Rmsd from ideal values	
Bond lengths (Å)	0.003
Bond angles (°)	0.55
Ramachandran plot[e]	
Favored	98.9
Outliers	0
Coordinate error (Å)[e]	0.34

[a] Numbers in parentheses are for the highest resolution shell.
[b] $R_{merge} = \sum_{hkl}(\sum_i(|I_{hkl,i} - <I_{hkl}>|))/\sum_{hkl,i}<I_{hkl}>$, where $I_{hkl,i}$ is the intensity of an individual measurement of the reflection with Miller indices h, k and l, and $<I_{hkl}>$ is the mean intensity of that reflection. Calculated for $I > -3\sigma(I)$.
[c] $R_{cryst} = \sum_{hkl}(||Fobs_{hkl}| - |Fcalc_{hkl}||)/|Fobs_{hkl}|$, where $|Fobs_{hkl}|$ and $|Fcalc_{hkl}|$ are the observed and calculated structure factor amplitudes.
[d] R_{free} is equivalent to R_{cryst} but calculated with reflections (5%) omitted from the refinement process.
[e] Calculated with the program MOLPROBITY (Davis et al., 2007). The coordinate error is the maximum likelihood based coordinate error.

The ring-like conformation found in the crystals of unliganded yImpβ is somewhat similar to exportins CRM1 (Dong et al., 2009a, 2009b; Monecke et al., 2009; Petosa et al., 2004) and unliganded Cse1 (Cook et al., 2005) (Figure 1A). The interactions that mediate ring formation are not conserved between Impβ and Cse1, which shows contacts between repeats H1-3 and H14-16. Because of the different roles in import and export, the physiological significance of these compacted structures is unlikely to be the same. In exportins, RanGTP and cargo binding in the nucleus cooperate to open up the structure and assemble the export complex (Cook et al., 2005; Dong et al., 2009a, 2009b; Petosa et al., 2004).

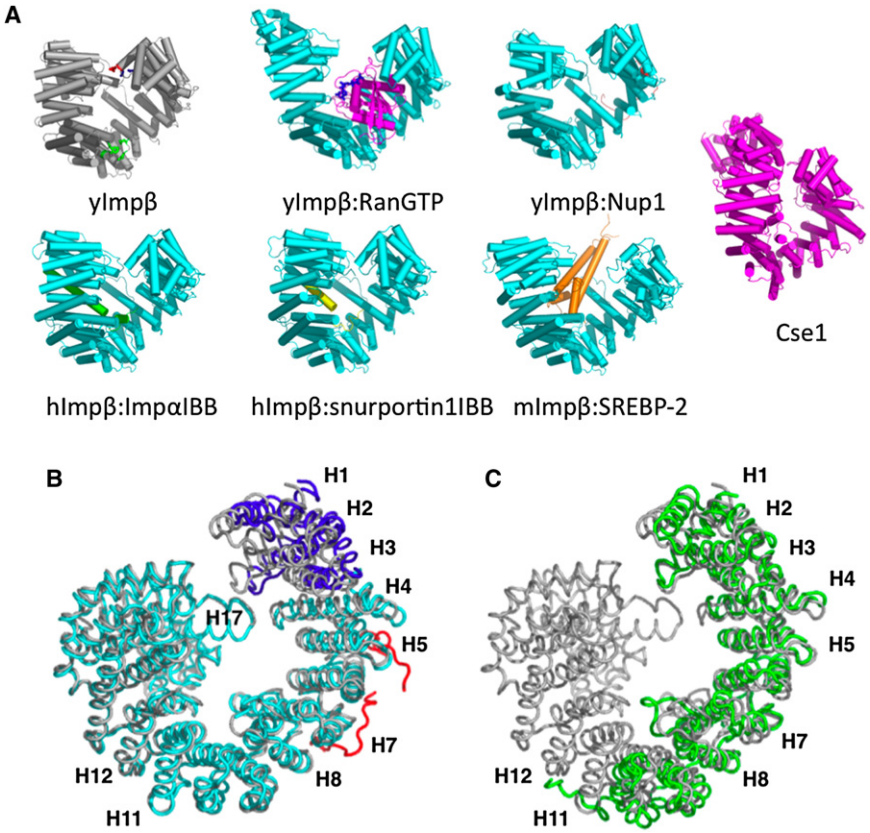

Figure 1. Comparison of yImpβ, Ligand-Bound Impβ and Cse1 Structures

(A) The structures are shown in cartoon representation in analogous orientation with cylinders representing α helices. yImpβ, crystal structure of unliganded yImpβ (gray). Residues targeted in mutagenesis studies are shown in stick representation and colored: red, Ser74 (HEAT repeat H2)/Glu737 (H17); blue, Asp167 (H4)/Asn738 (H17); green, Glu341 (H8)/Phe514 (H12) and Asp343 (H8)/Lys468 (H11). yImpβ:RanGTP, structure of yImpβ (cyan) bound to Ran (magenta) and GTP (blue in stick representation) (PDB ID 2bku) (Lee et al., 2005). yImpβ:Nup1, structure of yImpβ (cyan) bound to Nup1 (red) (2bpt; Liu and Stewart, 2005). hImpβ:ImpαIBB, structure of hImpβ (cyan) bound to the IBB domain of Impα (green) (1qgk; Cingolani et al., 1999). hImpβ:snurportin1IBB, structure of hImpβ (cyan) bound to the IBB domain of snurportin1 (yellow) (2q5d) (Mitrousis et al., 2008). mImpβ:SREBP-2, mImpβ (cyan) bound to a dimer of SREBP-2 (orange; 1ukl) (Lee et al., 2003). Cse1, structure of unliganded Cse1 (magenta) (1z3h) (Cook et al., 2005).

(B) Superposition of the structures of unliganded yImpβ (gray) and yImpβ (cyan, HEAT repeats H1-H3 blue):Nup1p (red) complex (PDB ID 2bpt).

(C) Superposition of the structures of unliganded yImpβ (gray) and unliganded mImpβ fragment comprising residues 1–454 (green) (PDB ID 1gcj).

See also Figure S1.

Small-angle X-Ray Scattering Studies of S. cerevisiae and Mouse Importin-β

Previous SAXS studies indicated that mImpβ had an S-shaped conformation in solution (Fukuhara et al., 2004). We collected SAXS data to characterize the solution behavior of the yImpβ used in crystallization, and to compare it with mImpβ. The scattering patterns of both yImpβ and mImpβ display a shoulder at $q \approx 1\ nm^{-1}$ (Figure 2A), as seen previously for unliganded mImpβ, as well as β-karyopherins transportin and Xpo-t (Fukuhara et al., 2004). The radius of gyration R_g and the maximum dimension D_{max} inferred from the pair distance distribution function (P(r), shown in Figure 2B) by the program GNOM (Svergun, 1992) were found to be 39 and 120 Å for yImpβ and 45 and 145 Å for mImpβ, respectively. These results indicate that the average size of yImpβ in solution is larger than that seen in the crystals (calculated R_g = 33 Å, D_{max} = 91 Å), and smaller than for mImpβ. The low-resolution shapes modeled based on their scattering profiles (Figure 2C) show a coiled structure for both proteins, comparable to the S-like conformation seen previously (Fukuhara et al., 2004). yImpβ is more compressed along the superhelical axis than mImpβ.

The theoretical scattering profiles of previously solved yImpβ atomic models (Protein Data Bank [PDB] ID 3ea5, 2bku, 2bpt; binding partner coordinates removed) were calculated by the program CRYSOL (Svergun et al., 1995), and are shown in Figure 2D. These theoretical curves also exhibit a shoulder at $q \approx 1\ nm^{-1}$; however, they do not readily superimpose onto the experimental scattering pattern, clearly evident by large χ^2 values ($\geq$4.9). This suggests that the average shape of the molecule in solution does not correspond to any available crystallographic model. The program OLIGOMER (Konarev et al., 2003) was used to assess whether the scattering pattern for yImpβ could be better represented as a linear combination of multiple crystallographic structures. Using the calculated scattering intensities of the closed unliganded yImpβ and the more open yImpβ:RanGDP structure (PDB ID 3ea5, Ran coordinates removed), an improvement in the χ^2 value (= 4.3) was observed (using volume fractions of 3ea5 and unliganded yImpβ of 84.3% and 15.7%, respectively; Figure 2D). Including additional

Table 2. yImpβ Mutations

Mutation Predicted to Enhance Intramolecular Interactions	Interaction		Mutation Predicted to Disrupt Intramolecular Interactions
S74K	Ser74	Glu737	E737K
		Arg696	
	Asn738	Asp167	D167K
	Gly739		
F514K	Phe514	Glu341	E341A
	His466		
	Asp343	Lys468	K468D
	Pro340		

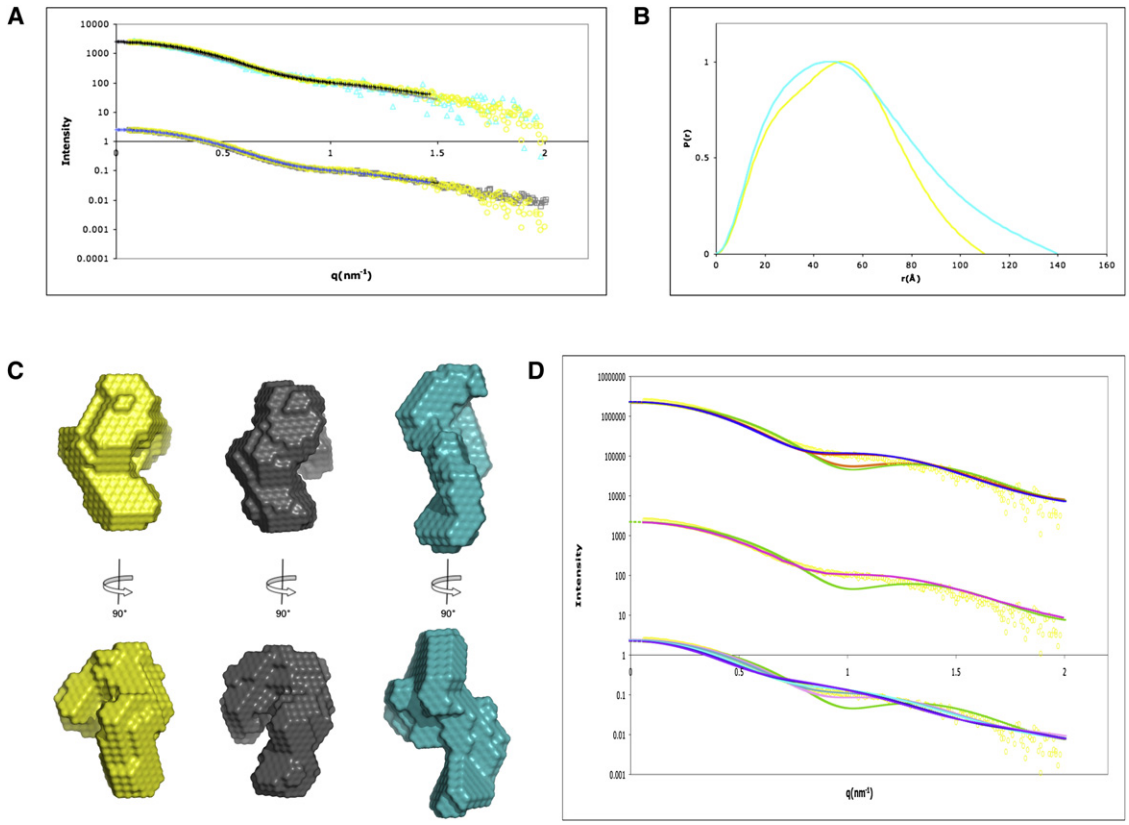

Figure 2. Small Angle X-ray Scattering Data

(A) The desmeared scattering curves of yImpβ (yellow circles), yImpβ S74K mutant (gray squares), and mImpβ (cyan triangles) are plotted as a function of the scattering vector q (nm^{-1}). The fit of the most probable model refined by DAMMIN (Svergun, 1999) for yImpβ (black), yImpβ S74K mutant (blue), and mImpβ (gray) is overlaid. The data have been displaced along the y axis for clarity.

(B) The distance distribution function, P(r) obtained from GNOM (Svergun, 1992), showing a D_{max} of 110 Å for yImpβ (yellow) and 140 Å for mImpβ (cyan). The forward scattering intensity, I(0), was used to calculate the molecular weight of the proteins in solution, yielding 107 ± 25 and 98 ± 25 kDa for the yeast and mouse proteins, respectively.

(C) Low-resolution shapes of yImpβ (yellow), yImpβ S74K mutant (gray), and mImpβ (cyan) calculated from the desmeared SAXS data by the program DAMMIN (Svergun, 1999). Ten dummy atom models were averaged by DAMAVER (Volkov and Svergun, 2003), and the averaged model was further refined in DAMMIN. The orientations are not related to those in Figure 1.

(D) Calculated scattering curves of yImpβ atomic models were calculated using the program CRYSOL (Svergun et al., 1995) and are shown overlaid onto the experimental scattering profile of yImpβ (yellow circles). The profiles have been displaced along the y axis for clarity. Top: ligand-bound yImpβ atomic models with binding partner coordinates removed (PDB ID 2bku, blue; 3ea5, red; 2bpt, orange; unliganded yImpβ, green). Middle: the fit corresponding to an 84.3% contribution from 3ea5 (Ran coordinates removed), and a 15.7% contribution from unliganded yImpβ as calculated by the program OLIGOMER (Konarev et al., 2003), shown in pink. The calculated scattering curve of the unliganded structure is shown in green for comparison. Bottom: calculated scattering profiles from MD simulations of unliganded yImpβ (R_g value of 3.4 nm, pink; 3.6 nm, teal) and from a previous MD study (Zachariae and Grubmuller, 2008) (R_g values of 3.9 nm, cyan; 4.2 nm, navy blue; 4.4 nm, purple).

See also Figure S2.

structures of yImpβ (PDB ID 2bku and 2bpt) did not result in a decrease of χ^2 value, presumably because of the high similarity of these conformations to those seen in 3ea5, and the unliganded yImpβ. However, a slight improvement in the χ^2 value (to 4.0) was achieved through the addition of the scattering intensity calculated from the crystal structure of mImpβ (PDB ID 1ukl, coordinates of SREBP-2 removed) (using volume fractions of 3ea5, unliganded yImpβ and 1ukl of 56.5%, 7.3%, and 36.2% respectively). Nonetheless, only χ^2 values <2 are considered meaningful using this analysis. Altogether, the data suggest that the yImpβ is most likely sampling a range of conformations in solution, which favors a more elongated state than seen in the crystal. However, the spectrum of conformations that yImpβ adopts in solution cannot simply be described as a combination of the currently available crystal structures.

Molecular Dynamics Simulations of S. cerevisiae Importin-β

Previous MD simulations indicated that unliganded Impβ was able to undergo rapid and large conformational changes in solution (Zachariae and Grubmuller, 2008). We used MD to test if the structure of unliganded yImpβ observed in the crystals was likely to persist in solution. Starting the simulation with the structure observed in the crystal, rapid conformational changes occurred during the early stages of the simulations that led to a marked

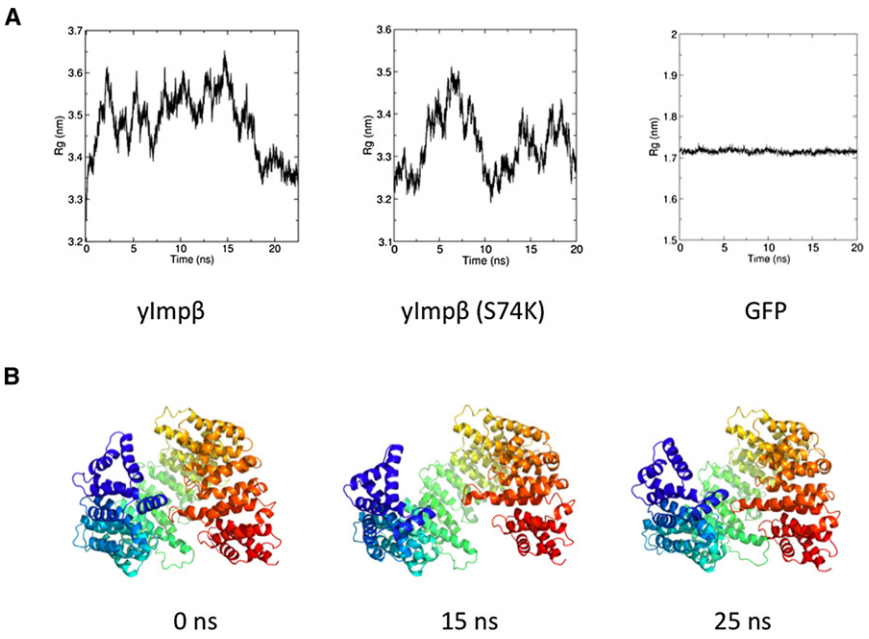

Figure 3. Molecular Dynamics Simulations

(A) Evolution of radius of gyration of during molecular dynamics simulation. Left, yImpβ. The starting condition of the simulation was the crystal structure. The observed tendency toward larger R_g values during the first part of the simulation indicates an evolution toward a more elongated structure in solution; however, another compact state is regained around t = 17 ns, together with a transient reformation of the original sequence-distal contacts. Middle, yImpβ S74K mutant. Right, GFP.

(B) Snapshots of structures during the MD simulation of yImpβ. Left, the starting compact conformation corresponding to the crystal structure. Middle, an extended conformation after 15 ns of simulation. Right, a compact confiormation after 25 ns of simulation.

elongation of the protein (during the first 2.5 ns, R_g increased from 32.5 to 36 Å, and the Cα rmsd relative to the initial structure to 6 Å; Figure 3). The sequence-distal contacts between H2/4 and H17 were not preserved. After subsequent contraction (t∼3 ns, R_g = 34 Å) and expansion (t = 15 ns, R_g = 36.5 Å, rmsd = 8 Å), yImpβ started to enter into another phase of contraction after 15 ns and reformed a compact state with a number of loose sequence-distal contacts between H2/4 and H17, as well as H7 and H18/19. The structure after t∼22 ns resembled the crystal structure (rmsd∼3 Å), and appeared to be stable over the course of several ns.

The SAXS profiles from a number of the MD conformations were calculated using CRYSOL (Svergun et al., 1995; Figure 2D). Additionally, the SAXS curves of more elongated structures from previous simulations were also calculated (Zachariae and Grubmuller, 2008). Although some of the MD conformations showed an improved fit to the solution scattering curve, indicated in a decrease in χ^2 (values ranging from 3.2 to 7.8) compared with the crystallographic models (see previous section; χ^2 values $\geq$4.9), no single conformation could adequately describe the measured scattering profile of yImpβ. These results further support the interpretation that Impβ samples a range of conformations in solution.

Mutational Analysis of S. cerevisiae *Importin-β*

To assess the in vivo requirement for the amino acids that may stabilize the circular arrangement of unliganded yImpβ found in the crystals, we engineered amino acid substitutions in the regions of H2, H4, and H17 (S74K, E737K, and D167K). As a control, we also engineered analogous mutations in H8, H11, and H12 (F514K, E341A, and K468D; Figure 1 and Table 2; see Figure S1A available online). The mutations were designed to either disrupt or stabilize the observed structure. Several of these residues are conserved in hImpβ (D167 is conserved and E737, E341 and K468 conserve the charge) (Figure S1B). A plasmid shuffle assay was used to determine if the amino acid substitutions affect the essential function of yImpβ in vivo. *ΔRSL1* cells, which lack the gene encoding yImpβ but contain a yImpβ maintenance plasmid, were transformed with vector alone or plasmid encoding wild-type or mutant yImpβ. Cells were plated on control plates or on plates containing the drug 5-FOA (Boeke et al., 1987), which removes the maintenance plasmid and leaves the yImpβ mutant as the only cellular copy of yImpβ (Figure 4A). None of the substitutions significantly impacted growth and therefore yImpβ function. Growth curve analysis also did not show significant differences in growth (not shown). All proteins were expressed at similar level as wild-type yImpβ-GFP (Figure 4B). To verify that amino acid substitutions within yImpβ can indeed disrupt protein function, a control variant of yImpβ (L329T, L330T, L332L, L333T) was assayed by plasmid shuffle (Figure 4C). Cells expressing this variant yImpβ as the only copy of yImpβ were unable to grow, consistent with previous studies, which show that a even single amino acid change within yImpβ can impair its function in vivo (Iovine and Wente, 1997).

We further examined whether any of the amino acid substitutions had an impact on transport of cargo proteins into the nucleus, by assessing the steady-state localization of the model classical NLS-containing cargo SV40TAgNLS-GFP-GFP or GFP-GFP alone as a control, in cells containing either wild-type or mutant yImpβ as the only copy of yImpβ (Figure 5A). Cells were costained with Hoechst to verify the position of the nucleus (data not shown). The double GFP tag was used to minimize passive diffusion through nuclear pores, though some degree of nuclear localization of GFP-GFP was expected (Hodel et al., 2006). For each yImpβ mutant, GFP-GFP alone localized throughout the cell and SV40TAgNLS-GFP-GFP showed significant steady-state nuclear localization, indicating that the substitutions do not significantly impair yImpβ function in the classical nuclear import pathway. Furthermore, the interaction between yeast Impα (Kap60/Srp1) and the yImpβ variants is not significantly altered, because the heterodimeric import receptor must form for classical import to occur. There may be a slight decrease in the nuclear localization of the NLS reporter in the K468D mutant, but attempts to confirm through counting cells

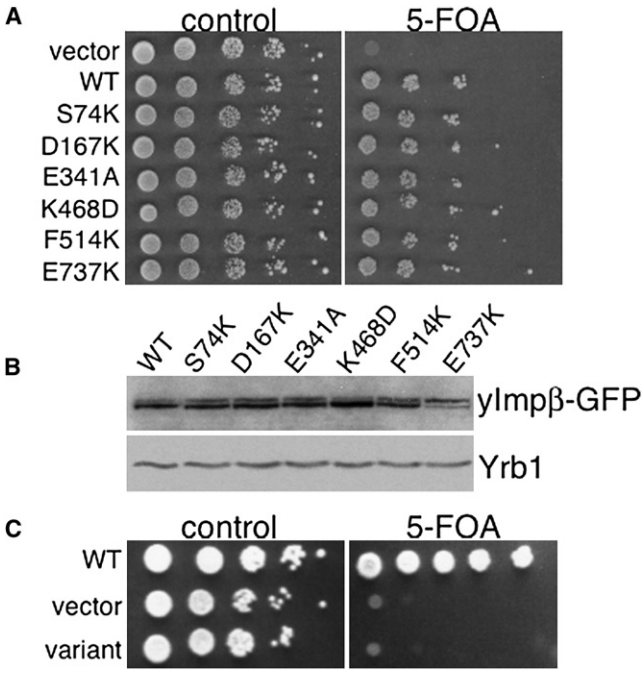

Figure 4. Functional Analysis of the yImpβ Mutants In Vivo

(A) *S. cerevisiae* cells deleted for the endogenous yImpβ (*ΔRSL1*) but containing a yImpβ maintenance plasmid (ACY208) were transformed with vector alone (negative control) or a plasmid encoding wild-type (positive control) or mutant yImpβ. Cells were plated on control plates or on plates containing the drug 5-FOA and grown at 25°C. 5-FOA removes the maintenance plasmid and leaves the yImpβ mutant as the only cellular copy of yImpβ.

(B) The level of each of the yImpβ-GFP variants expressed in wild-type cells (ACY192) was detected by immunoblotting with an anti-GFP antibody. Levels of a control protein, Yrb1, were monitored with an anti-Yrb1 antibody (Schlenstedt et al., 1995) to ensure that an equal amount of total protein was loaded in each lane.

(C) *S. cerevisiae* cells deleted for the endogenous yImpβ but containing a yImpβ maintenance plasmid were transformed with a plasmid encoding wild-type yImpβ, vector alone, or variant yImpβ, serially diluted, and spotted on control or 5-FOA plates.

See also Table S1.

in a double-blind experiment showed no statistically significant difference.

Finally, a kinetic import assay was used to determine if the initial rate of NLS-cargo import was altered. Cells containing mutant or control yImpβ as the only copy and expressing either GFP-GFP or SV40TAgNLS-GFP-GFP were incubated with azide and 2-deoxy-glucose, which deplete the cell of energy and cause redistribution of any nuclear cargo throughout the cell (Shulga et al., 1996). After washing out the inhibitors, import kinetics were measured by assessing the percentage of cells with nuclear accumulation of the reporter over time (Figure 5B). The rate of initial import of the NLS-reporter was similar in all cells analyzed (including the K468D mutant).

To obtain additional evidence of the effect the mutations on the structure of yImpβ, we performed SAXS measurements and MD simulations on the S74K mutant using the same conditions as for wild-type yImpβ. Consistent with the functional experiments, the mutant behaved very similar to wild-type (Figures 2 and 3).

Jointly, the results of mutagenesis, SAXS and MD studies are consistent with the idea that the structure seen in the crystals of unliganded yImpβ is one of a spectrum of structures that are in rapid equilibrium in solution. Although the computer-intensive nature of MD simulations allows only relatively short timescales to be examined, the present simulations suggest that elongated states are likely to be favored in solution, but that a local energy minimum stabilizes the compact structure seen in the crystal.

Quantitative Analysis and Molecular Basis of Impβ Flexibility

Translation/Libration/Screw Analysis of Importin-β Structures

Another way in which the flexibility of the different Impβ structures can be assessed is to analyze correlations in the molecular motion of individual residues. In crystal structures, this motion is modeled as the B factor and can be due to static disorder or dynamic motion. However, for vitrified crystals examined at 100 K, this parameter is probably describing primarily static disorder that is related to the flexibility of the molecule generating different conformations throughout the crystal prior to cooling. For crystal structures in the resolution range represented by the different Impβ studies (2.0–2.7 Å resolution), isotropic atomic B factors are usually employed in refinement because there are insufficient observations to model anisotropic disorder. However, groups of residues often form comparatively rigid blocks, and so the anisotropic disorder can be modeled for the entire group as a whole, using the translation/libration/screw (TLS) formulation (Painter and Merritt, 2006). This approach is most applicable to multidomain proteins. However, although Impβ structures are probably better represented as a continuous flexible domain, the anisotropic disorder due to flexing of such a structure can be approximated by employing a large series of small segments analogous to the segmented chain models that are frequently used to describe motions of chains in polymer physics (see, for example, Rubinstein and Colby, 2004). Using a successively larger number of segments will produce an increasingly close approximation to the anisotropic disorder of the molecule as a whole, albeit using too large a number of segments will result in the structure becoming overrefined, as the number of parameters exceeds the number that can be described by the number of observations (overrefinement is indicated by an increase in free R factor). Previous work (Cansizoglu and Chook, 2007) used only three such TLS domains selected automatically (Painter and Merritt, 2006) to assess the flexibility of Impβ. However, some caution is necessary because applying TLS refinement to a structure such as Impβ is not entirely straightforward, because the implicit assumption that the structure is composed of a number of completely independent domains is unlikely to be strictly correct. Moreover, errors will be introduced at the boundaries between successive segments, although, provided the fluctuations are relatively small, these errors should not dominate the analysis. A plot of the Cα B factors along yImpβ (Figure 6A) shows a distinctive fluctuation, indicative of there being some degree of correlation between B factors locally, consistent with a TLS-based analysis being a useful approximation to the anisotropic disorder of the molecule. We assessed the degree to which successively fine TLS regions approximate the molecular disorder by monitoring the

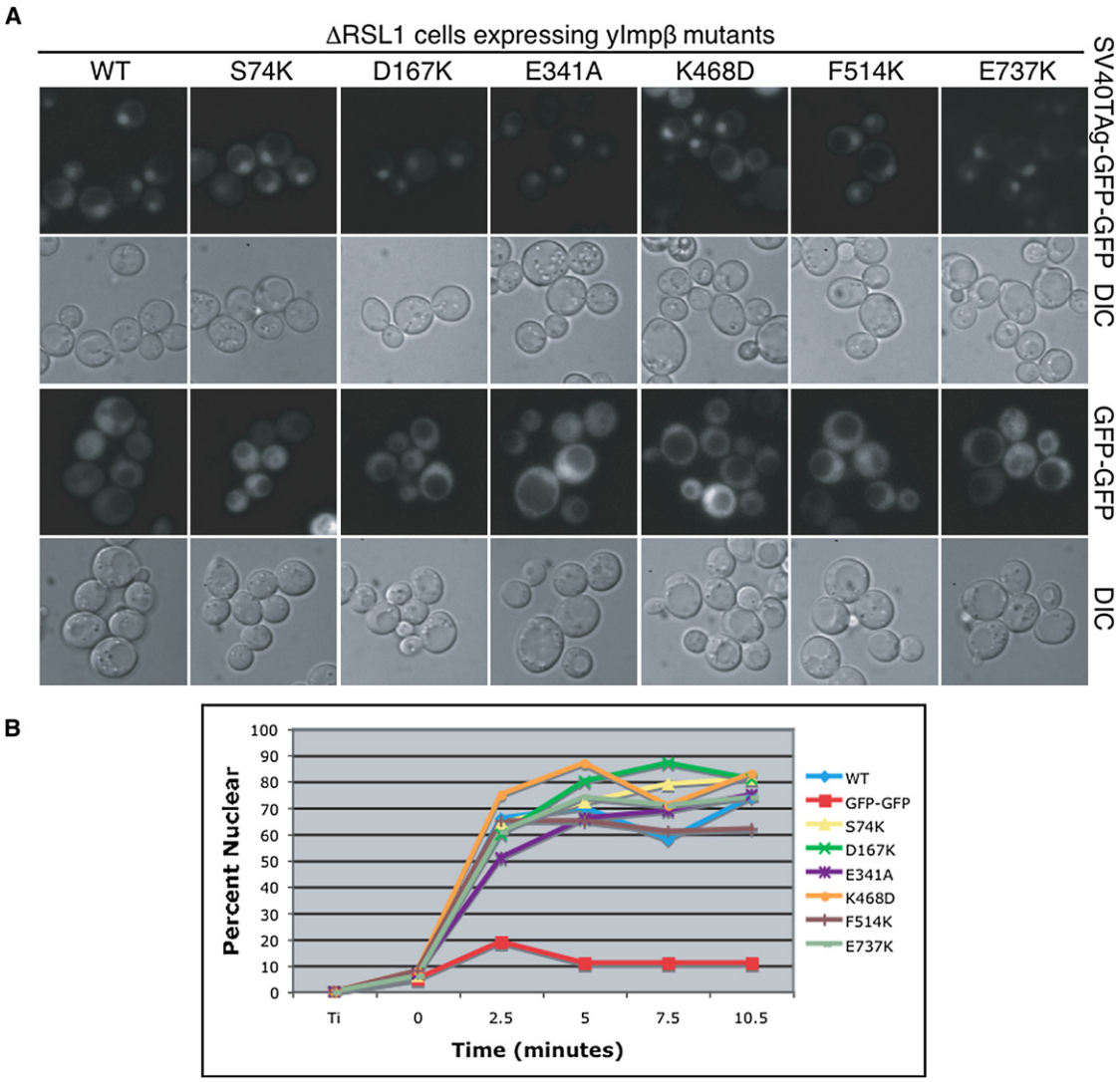

Figure 5. Functional Analysis of cNLS Cargo Import

Cells expressing yImpβ mutants or control wild-type yImpβ as the sole copy of yImpβ were transformed with plasmids encoding either SV40TAgNLS-GFP-GFP (pAC1065) or GFP-GFP (pAC1069) under the control of the inducible *MET25* promoter. Cells were grown overnight in selective media, induced in media lacking methionine, and incubated overnight prior to localization studies (A) or kinetic import assays (B). (A) The GFP fusion proteins were localized by direct fluorescence microscopy. The corresponding differential interference contrast (DIC) images are shown. (B) The initial import kinetics for nuclear import of NLS-cargo in cells expressing yImpβ mutants or control wild-type yImpβ as the only copy of Impβ in the cell were measured by assessing the percentage of cells with nuclear accumulation of SV40TAgNLS-GFP-GFP every 2.5 min over a 10 min time course (Shulga et al., 1996). As a control, the initial import rate for GFP-GFP was examined in wild-type cells. The percentage of cells with nuclear accumulation is plotted against time, with T_i denoting the initial time point taken before the cells were resuspended in media to initiate nuclear import.

free R factor during the TLS refinement. As the TLS model approximates the molecular disorder increasingly closely, the free R factor should decrease as the refined model becomes more consistent with the diffraction data, whereas overrefinement would be flagged by an increase in the free R factor. When the 2.4 Å resolution unliganded yImpβ structure was refined in this way, using TLS regions generated by the http://skuld.bmsc.washington.edu/~tlsmd/ website (Painter and Merritt, 2006), the free R factor decreased progressively as the molecule was divided into progressively smaller regions, until six to eight regions were employed. After this, further subdivision into smaller regions did not result in a decrease in the free R factor and indeed, it began to increase slightly indicating that the structure was becoming overrefined (Figure 6B). Moreover, when six segments were employed, the model was approximating the B factor fluctuations along the molecule reasonably well. TLS models based in individual HEAT repeats did not improve the free R factor over that obtained using six segments. We also applied this analysis to the refinement of the 2.0 Å resolution structure of the yImpβ:Nup1 complex (PDB ID 2bpt) (Liu and Stewart, 2005). For this higher resolution structure, the minimum R_{free} was obtained with 13–14 TLS segments

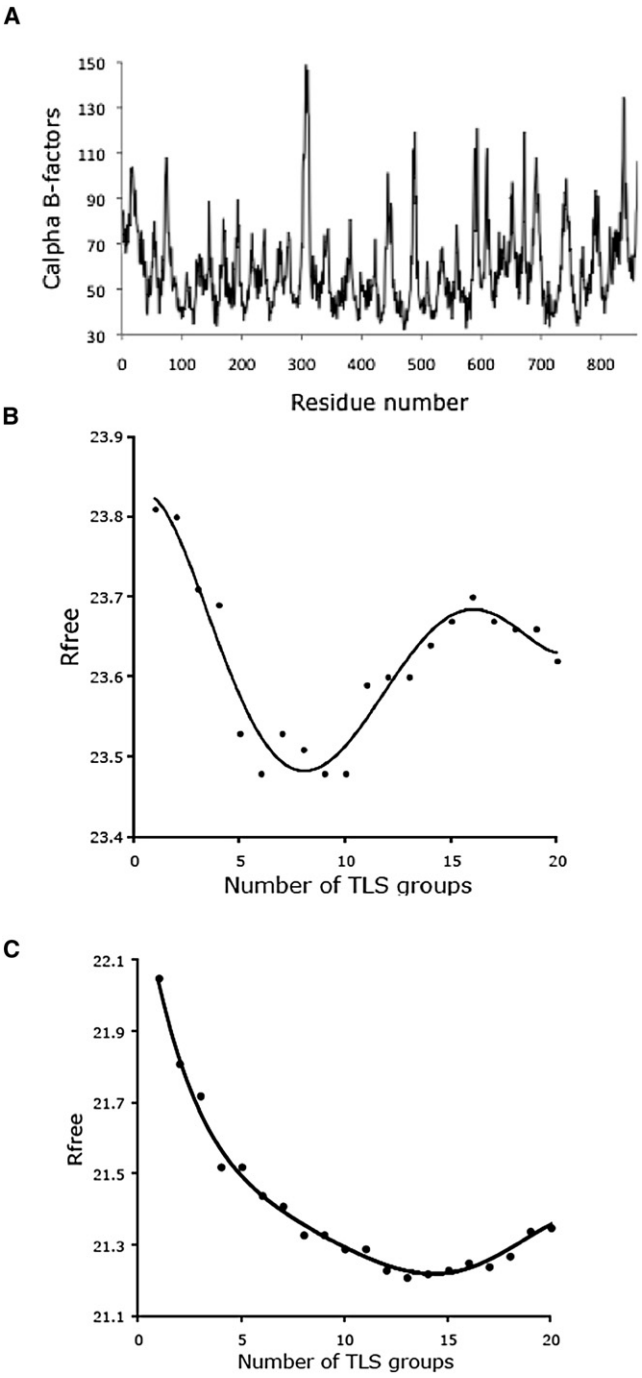

Figure 6. TLS Analysis of yImpβ Crystal Structure

(A) Variation of B factors along the yImpβ molecule. The periodic fluctuations and the overall shape of the plot are consistent with the molecule containing a number of segments that can be considered, to a first approximation, as rigid bodies for TLS refinement.

(B) Variation in R_{free} when different numbers of TLS groups were used to refine the 2.4 Å resolution yImpβ crystal structure. R_{free} reduces as progressively more TLS groups are added until six to eight groups are employed (these correspond to residues 1–130; 130–309; 310–442; 443–587; 588–699; and 700–-861 in the case of six groups). Adding further groups results in a small increase in R_{free} indicating that the structure may be becoming overrefined.

(C) Variation in R_{free} when different numbers of TLS groups were used to refine the 2.0 Å resolution yImpβ:Nup1 crystal structure (PDB ID 2bpt). R_{free} reduces as progressively more TLS groups are added until 13–14 groups are employed (these correspond to residues 1–77; 78–166; 167–172; 173–274; 275–391; 392–438; 439–546; 547–592; 593–670, 671–690; 691–765; 766–831; and 832–861 in the case of 13 groups). Adding further groups results in a small increase in R_{free} indicating that the structure may be becoming overrefined.

(Figure 6C), consistent with the greater number of observations enabling a more precise description of the anisotropic disorder to be made. Thus, for refinement of the structures of both the unliganded yImpβ and its complex with Nup1, a progressively larger number of TLS blocks gave a progressively closer description of the motion of the molecule until a resolution-dependent limit was reached, after which the structure started to become overrefined. The overrefinement most probably resulted from the number of parameters (in this case, the number of segments) exceeding the limit set by the number of observations in the structure factor data set. This suggests that an even greater number of blocks would be appropriate, were it possible to obtain a higher resolution data set that contained a greater number of observations. Thus, this analysis tends to support approximating the motion of yImpβ by a segmented chain model with a large number of segments, which, in the limit, approaches a continuously flexible chain or at least one in which the individual HEAT repeats or their constituent helices formed the segments. Overall, therefore, the TLS analysis was consistent with the yImpβ molecule having a relatively continuously flexible conformation rather than being constructed from simply two or three rigid domains separated by very flexible hinges.

Quantitative Geometric Analysis

To perform a systematic analysis of HEAT repeats in different Impβ structures, we used an approach similar to that used recently for leucine-rich repeat (LRR) proteins (Bublitz et al., 2008). The orientation of each repeat was defined with respect to the preceding repeat using three angles: curvature, twist, and lateral bending. In the LRR study, each repeat was represented by a triangle based on three chosen Cα positions (Bublitz et al., 2008). To increase the general applicability to different repeats and the ability to automate the calculations, we instead defined three principal axes for each repeat based on the Cα positions of all residues in a repeat, and calculated the interrepeat angles based on the principal axes of two adjacent repeats (Figure 7).

Analyses indicate that there is a remarkable conservation of the interrepeat angles between human, mouse, and yeast Impβ, which can therefore be compared directly. This conservation suggests that the particular interrepeat geometry is functionally critical and is consistent with an extensive interface holding adjacent repeats together. The results will be illustrated on six representative structures, which cluster qualitatively in four distinct patterns of interrepeat angles: (i) yImpβ and Nup1-p:yImpβ; (ii) Impα and snurportin1 IBB:hImpβ; (iii) RanGT-P:yImpβ; and (iv) SREBP-2:mImpβ (Figure 7C). For comparison, a similar analysis performed on structures simulated by MD calculations is shown in Figure S2. There is a pronounced irregularity of the distribution of interrepeat angles along the chain, as compared with LRR proteins (Bublitz et al., 2008). This may reflect a higher sequence variation between HEAT repeats, and the presence of a β sheet in the LRR structure that may limit the structural variation as compared to helix-helix contacts

featured in HEAT repeats. The irregularity is higher than changes imposed by binding of different partners. The interrepeat angle variation does not correlate with repeat sequence variation. The curves show regions of greater variability at HEAT repeats H3-7 and H12-16. These regions correlate with the areas identified as hinges in previous studies, such as hinges suggested at H13 and H14-15 (Cansizoglu and Chook, 2007) and flexible hot spots at H4-5 and H14-15 (Zachariae and Grubmuller, 2008). Conversely, the more rigid areas with least variability in interrepeat angles between the different proteins correspond to repeats H2, H6-9, and H11. The variability pattern is also consistent with the segments defined in the TLS analysis (Figure 6). The results are again more consistent with gradual flexing over a larger region in Impβ, rather than two or three rigid domains separated by hinges.

The regions of greater variability identified above correlate somewhat with the regions that form contacts with binding partners. For example, RanGTP interacts with yImpβ in three areas of the protein (H1-4, H7-8, and H12-15). The variation from other structures is most pronounced at the edges of these interacting regions, at H4-5 and H13-17. The inspection of the molecular details responsible for the interrepeat angle changes further supports the observation that the conformational changes are not localized to specific hinges but a result of accumulated small changes throughout the solenoid, as illustrated below on a few specific examples. As the first example, unliganded and RanGTP-bound yImpβ show substantial differences in curvature at H4, as a result of the movement of the A helices on the convex face of the solenoid in H4 and H5 further apart in the RanGTP form (Figure 8A). This movement is accompanied by smaller relative rotations of the A helices (mostly affecting the lateral bending), to accommodate a different packing arrangement of the side chains between the A helices, and may be driven by electrostatic interactions of RanGTP with the A helices. As the second example, the same pair of structures exhibits a difference in lateral bending angle between H14 and the adjacent repeats (Figure 8B). Here, the major difference is localized to the B helices on the concave face of the solenoid. The movement is coupled with a rotation of the large side chains of Phe613, Phe619, and Tyr620 on the B helix of H14, influenced by the interactions with RanGTP. In the final example, the two IBB domain-bound structures show differences in the same region, presumably induced by the differences in the Impα and snurportin1 IBB domain sequences and therefore the mode of interaction in this region (e.g., the interaction with Arg28 in Impα versus Gln40 in snurportin1; Figure 8C).

Conclusions

Flexibility and dynamics represent an important dimension of protein function, characterization of which usually requires the use of a combination of techniques and approaches (Cowieson et al., 2008). In terms of flexibility, solenoid structures fall in between globular structured proteins and intrinsically unstructured proteins (Wright and Dyson, 1999); while the hydrophobic core provides stability typical of a folded protein, the lack of sequence-distal contacts in the structure can allow higher flexibility (Kobe and Kajava, 2000). Although conformational changes in large structured proteins are usually assumed to involve movement of rigid domains around a small number of hinges (Qi et al., 2005), our results indicate that this is not the case in Impβ.

In summary, our results are consistent with Impβ being an inherently flexible molecule, which performs its functions by taking advantage of conformational transitions resulting from cumulative small structural changes along the length of the solenoid. Such continuous flexing can store internal energy much more efficiently than movements of rigid domains around flexible hinges. Our results may have general implications for solenoid proteins, which use their structural properties to carry out their cellular functions, their inherent flexibility allowing the specific binding of a single protein to a number of binding partners at different stages of a pathway. This flexibility combined with the storage of internal mechanical energy can generate a gradation of affinities to orchestrate the appropriate sequence of binding reactions in the cell.

EXPERIMENTAL PROCEDURES

Protein Expression and Purification

Full-length GST-yImpβ and GST-mImpβ were expressed in *Escherichia coli* strain BL21(DE3)pLysS and purified by glutathione affinity chromatography (Forwood et al., 2008; Roman et al., 2009). The GST fusion-tag was cleaved using thrombin and removed by size exclusion chromatography. Fractions containing the purified recombinant yImpβ were passed through glutathione-Sepharose affinity matrix to remove residual traces of GST and uncleaved GST-Impβ. The protein was concentrated to 40 mg/ml and stored in 20 mM Tris (pH 7.4), 50 mM NaCl at −80°C.

Crystal Structure Analysis

Crystallization and diffraction data collection are described by Roman et al. (2009). Raw data were autoindexed, integrated, and scaled using the HKL2000 package (HKL Research, Inc.). The crystals displayed $P2_1$ symmetry, with unit cell dimensions of a = 58.17 Å, b = 127.25 Å, c = 68.52 Å; β = 102.23°. The crystals are similar to the crystals of the yImpβ:Nup1 complex (Liu and Stewart, 2005), which displayed the same symmetry and unit cell dimensions of a = 58.08 Å, b = 125.97 Å, c = 69.35 Å; β = 110.2°. The asymmetric unit contained one yImpβ molecule. Initial phases were obtained by molecular replacement using Phaser (Storoni et al., 2004) and yImpβ from the yImpβ:Nup1p structure (Liu and Stewart, 2005) as a search model. Local rebuilding using COOT (Emsley and Cowtan, 2004) and refinement with REFMAC (Murshudov et al., 1997) from the CCP4 program suite (CCP4, 1994) followed by Phenix (Zwart et al., 2008) and the use of TLS displacement model (Painter and Merritt, 2006) yielded a final model with good overall stereochemistry (Table 1). All molecular structure figures were prepared using PyMol (DeLano Scientific LLC).

Small Angle X-ray Scattering

Small angle X-ray scattering (SAXS) data were collected using an Anton Paar/Panalytical SAXSess system, with CuKα radiation from a sealed X-ray tube, line collimation and a CCD detector (Princeton Instruments). yImpβ and mImpβ were dialyzed overnight in 20 mM Tris 7.4, 125 mM NaCl, 10 mM DTT at 4°C. SAXS measurements were collected at 20°C at a concentration of 2–5 mg/ml, in a 1 mm silica capillary. To monitor for radiation damage, two to six successive 15 min exposures were compared, and no differences in scattering intensity were seen for either protein, suggesting that no structural changes had occurred. The scattering data were collected from q = 0.05 to 2.2 nm^{-1} and were reduced to remove the contributions from the dark current of the detector, scattering of the dialysis buffer and empty capillary. The data were further normalized to absolute intensity using pure water as a calibration standard. The indirect transform program GNOM (Svergun, 1992) was used desmear the scattering profiles and evaluate the pair distance distribution function p(r) and the maximum size D_{max}. The radius of gyration, R_g, and the forward scatter, I(0), was determined from the second and zeroth moments of P(r), respectively, as well as the maximum linear dimension of the particle, D_{max}. Ten dummy atom models were generated by the program DAMMIN

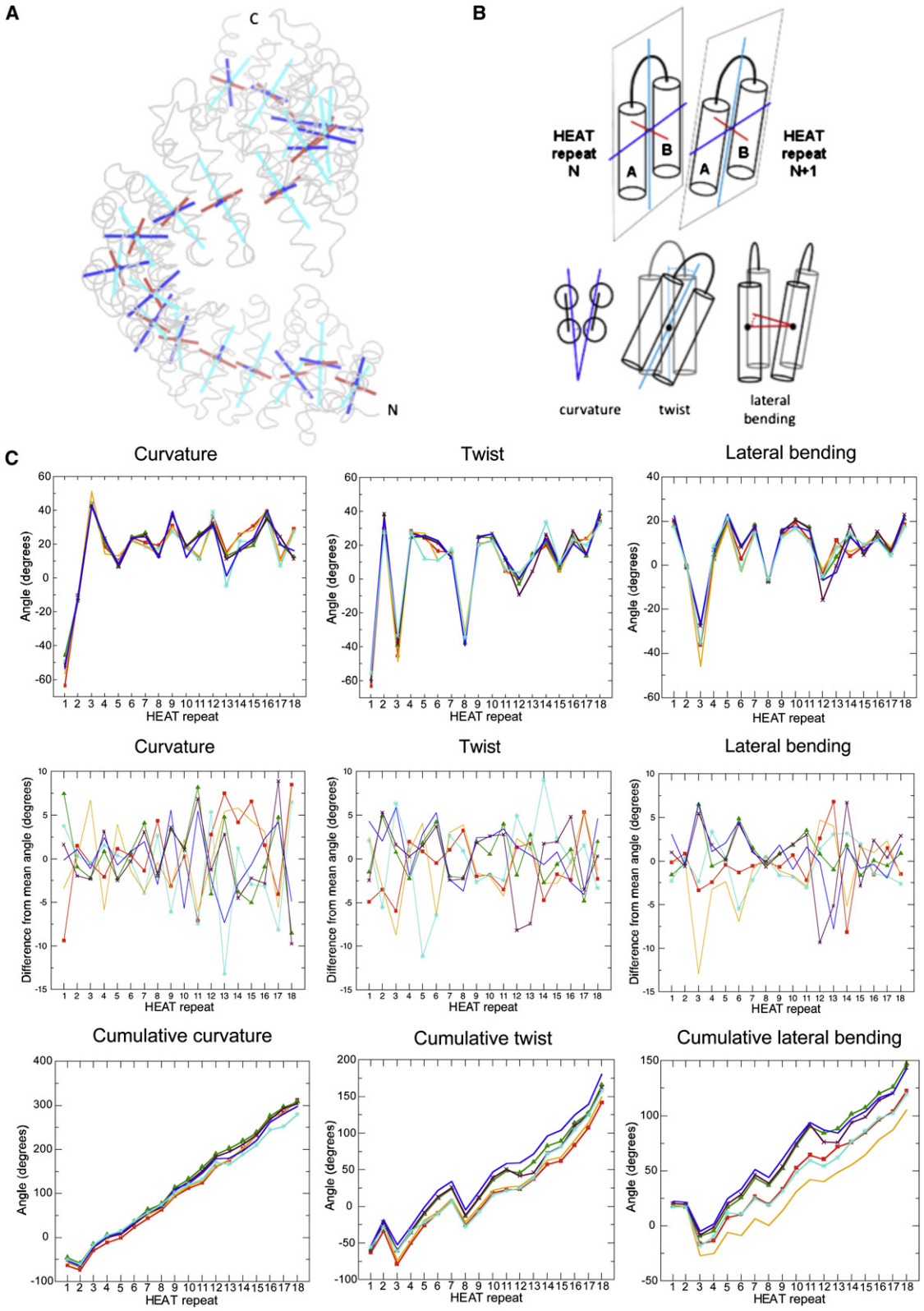

Figure 7. Variation of Interrepeat Angles between Successive HEAT Repeats

(A) Principal axes in successive repeats, shown in the structure of mImpβ (shown as ribbon diagram in gray) from the SREBP-2 complex as an example. Axis *P1* is the axis perpendicular to the helices in the plane of the repeat (blue); axis *P2* is the axis parallel to the helices in the plane of the repeat in individual repeats (cyan); and axis *P3* is the axis perpendicular to axes *P1* and *P2* (red).

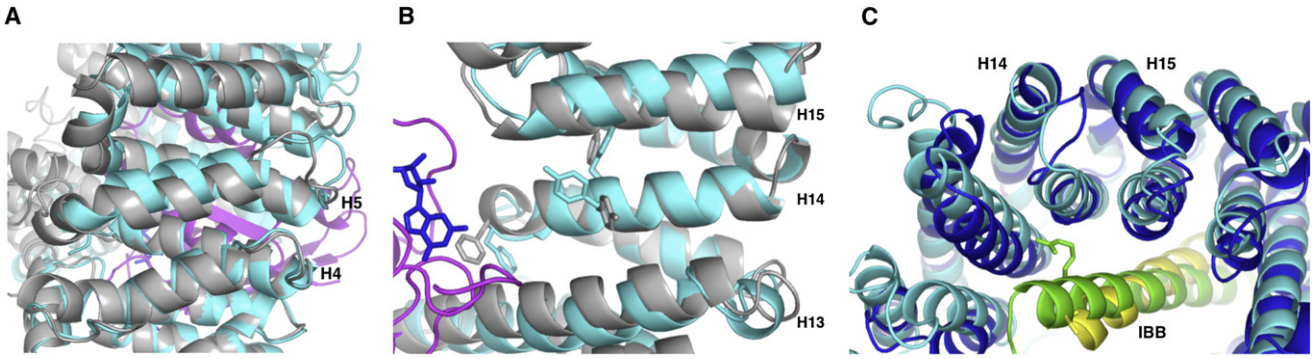

Figure 8. Molecular Basis of Interrepeat Angle Variation

(A) Movement in the region of HEAT repeats H4 and H5 when structures of yImpβ (gray) and yImpβ (cyan):Ran (magenta):GTP (blue) complex (PDB ID 2bku) are compared. H4 was used in the superposition. The structures are shown in cartoon representation, with GTP in stick representation.

(B) Movement in the region of HEAT repeat H14 when the structures of yImpβ (gray,) and yImpβ (cyan):Ran (magenta):GTP (blue) complex (PDB ID 2bku) are compared. H14 was used in the superposition. The structures are shown in cartoon representation, with GTP and side chains of Phe613, Phe619, and Tyr620 in stick representation.

(C) Movement in the region of HEAT repeat H14 when the structures of hImpβ (cyan) bound to the IBB domain from Impα (green) (PDB ID 1qgk) and hImpβ (blue) bound to the IBB domain from snurportin1 (yellow) (PDB ID 2q5d) are compared. H14 was used in the superposition. The structures are shown in cartoon representation, with the side chains of Impα IBB domain Arg28 and snurportin1 IBB domain Gln40 in stick representation.

(Svergun, 1999) using data in the range up to s = 1.5 nm^{-1} and the models were aligned using the program SUPCOMB (Kozin and Svergun, 2001). The program DAMAVER (Volkov and Svergun, 2003) was then used to construct the average model of all reconstructions and contoured at the 95% confidence level. The averaged model was then further refined using the generated damstart.pdb file as an input into DAMMIN (Konarev et al., 2006). Theoretical scattering curves of crystallographic atomic models were computed using CRYSOL (Svergun et al., 1995). The program OLIGOMER (Konarev et al., 2003) was subsequently employed to calculate the volume fractions of a mixture of several distinct crystallographic conformations, to give the best fit to the experimental curve.

Molecular Dynamics Simulations

The crystal structure of yImpβ was immersed in a dodecahedral box with box vectors of 14.9 nm, filled with TIP4P water molecules (Jorgensen et al., 1983), and Na^+/Cl^- ions according to an ionic strength of 0.15 M. After a short energy minimization, the system (size ~310,000 atoms) underwent an equilibration phase of 1 ns length, in which position restraints were applied on the heavy atoms of the protein. A production run of ~23 ns length followed, in which the temperature and pressure were kept constant by weak coupling to a temperature bath of 310 K and a pressure of 1 bar, respectively. Long-range electrostatic interactions were calculated using the particle-mesh-Ewald method (Darden et al., 1993); short-range electrostatic interactions and van der Waals interactions were calculated explicitly up to a cutoff distance of 1 nm. The time-step used was 2 fs, and all bond lengths were constrained using the LINCS algorithm (Hess et al., 1997). The energy minimizations and molecular dynamics trajectories were calculated using the OPLS-all atom force field (Jorgensen et al., 1996) in Gromacs version 3.3 (Lindahl et al., 2001).

Quantitative Geometric Analysis

The analysis of angles describing curvature, twist, and lateral bending between successive pairs of HEAT repeats was performed using an assignment of principal axes in individual repeats. The axes were obtained by a principal component analysis of the positions of Cα atoms in helical environments of a respective helix pair. Curvature is the angle between eigenvectors (ev) 2 of HEAT repeats N and N+1, projected onto a reference plane spanned by ev 3 and ev 2 of HEAT repeat N+1; twist is the angle made by ev 1 of HEAT repeats N and N+1, projected onto a reference plane spanned by ev 1 and ev 2 of repeat N+1; and lateral bending is the angle between ev 3 of HEAT repeats N and N+1, projected onto a plane spanned by ev 1 and ev 3 of helix pair N+1 (Figure 7). Our method is generally applicable to solenoid proteins, as the principal axes of repetitive motifs can be defined without the need for specifically conserved sequence positions, and also independent of secondary structure elements such as α helices. The program used for our geometric analysis (CuTLat: curvature, twist, lateral bending) is available for use on the web server http://www.mpibpc.mpg.de/home/grubmueller/downloads/cutlat/index.html.

Functional Analysis of yImpβ Mutants

All chemicals were obtained from US Biological or Sigma unless noted otherwise. All media were prepared and all DNA manipulations were performed as described previously (Adams et al., 1997; Sambrook and Russel, 2001). All yeast strains and plasmids used in this study are described in Table S1. *RSL1* is the gene that encodes yImpβ (Kap95) in *S. cerevisiae*.

GFP-fusion proteins were localized in live *S. cerevisiae* cells using direct fluorescence microscopy on an Olympus BX60 epifluorescence microscope equipped with a Photometrics Quantix digital camera. To localize the yImpβ variants, wild-type cells (ACY192) expressing wild-type or variant yImpβ-GFP under its own promoter were grown overnight in selective media, diluted in fresh media, and grown for 3 hr to log phase prior to localization. To assess the functional impact of amino acid substitutions in yImpβ mutants for classical nuclear import, a cNLS import cargo or GFP-GFP was localized in *ΔRSL1* cells expressing wild-type *RSL1* (ACY208) or each yImpβ variant as the only cellular copy of yImpβ. Transformants were plated on plates containing 5-fluoroorotic

(B) Definition of the interrepeat angles based on the principal axes of successive repeats. The curving angle is the angle between the *P1* axes of successive repeats; the twist angle is the angle between the *P2* axes of successive repeats; and the lateral bending angle is the angle between the *P3* axes of successive repeats.

(C) Variation of interrepeat angles along the polypeptide chain. Top row: Curvature (left), twist (middle), and lateral bending angles (right panels) for the structures of yImpβ (red squares), yImpβ:RanGTP (cyan stars), yImpβ:Nup1p (yellow horizontal bars), mImpβ:SREBP-2 (blue circles), hImpβ:ImpαIBB (green triangles), and hImpβ:snurportin1IBB (magenta crosses) (see legend to Figure 1). Top row: curvature, twist, and lateral bending angles along the polypeptide chain. Middle row: differences from mean angles for curvature, twist, and lateral bending angles along the polypeptide chain. Bottom row: cumulative values along the polypeptide chain for curvature, twist, and lateral bending angles.

acid (5-FOA) (Boeke et al., 1987) to remove the maintenance plasmid and were transformed with a plasmid encoding either SV40TAgNLS-GFP-GFP (Hodel et al., 2006) (pAC1065) or a GFP-GFP control (pAC1069) under the control of the *MET25* promoter. Cells were grown overnight in selective media, washed once in dH_2O, resuspended in media lacking methionine to induce expression of the reporter proteins, and incubated overnight prior to localization studies.

Immunoblot analyses were performed essentially as previously described (Towbin et al., 1979). Wild-type cells (ACY192) transformed with plasmids encoding the yImpβ-GFP variants were grown to log phase, collected by centrifugation, and washed once with dH_2O and twice with cold PBSMT (PBS, 5 mM $MgCl_2$, 0.5% Triton X-100). Glass bead lysis was conducted in PBSMT in the presence of the protease inhibitors phenylmethylsulfonyl fluoride (PMSF; 0.5 mM) and PLAC (pepstatin A, leupeptin, aprotinin, chymostatin; 3 μg/ml each). Lysates were cleared by centrifugation and total protein concentration was assessed by the Bradford assay. Thirty micrograms of protein was resolved by SDS-PAGE, transferred to a nitrocellulose membrane, and probed with an anti-GFP antibody (1:3,000, rabbit) to detect the yImpβ-GFP proteins and an anti-Yrb1 antibody (1:50,000, rabbit; Schlenstedt et al., 1995) as a loading control.

The in vivo function of each of the yImpβ mutants was assessed using a plasmid shuffle technique (Boeke et al., 1987). For the plasmid shuffle, vector alone or plasmids encoding the wild-type or variant yImpβ proteins were transformed into *ΔRSL1* cells containing a wild-type *RSL1 URA3* maintenance plasmid (ACY208). Single transformants were streaked onto control ura- leu- glu plates or on selective leu- glu plates containing 5-FOA. Plates were incubated at 25°C. A variant of yImpβ containing four leucine (L329, L330, L332, L333)-to-threonine changes was employed as a control to impact yImpβ protein function.

The cNLS import assay was performed essentially as previously described (Hodel et al., 2006; Shulga et al., 1996). Cells containing the yImpβ variants as the only copy of yImpβ and expressing the SV40TAgNLS-GFP-GFP reporter protein were grown and induced. After collection by centrifugation, cells were pelleted, resuspended in glucose-free media containing sodium azide and 2-deoxy-D-glucose, and incubated at 30°C for 45 min. The cells were washed with ice-cold dH_2O, resuspended in glucose-containing media prewarmed to 30°C, and incubated at 30°C. Following resuspension, samples were removed every 2.5 min and imaged using direct fluorescence microscopy. At least 100 cells were analyzed for each time point. Cells were scored as "nuclear" if the nucleus was discernable, i.e., if the nucleus was brighter than the cytoplasm and if a nuclear-cytoplasmic boundary was visible.

ACCESSION NUMBERS

The atomic coordinates and structure factors have been deposited in the Protein Data Bank, www.rcsb.org (PDB ID 3ND2).

SUPPLEMENTAL INFORMATION

Supplemental Information includes two figures and one table and can be found with the article online at doi:10.1016/j.str.2010.06.015.

ACKNOWLEDGMENTS

We thank M Bublitz for help with the geometric analysis, and K. Jack, N. Cowieson, and A. Whitten for help with SAXS. We acknowledge the use of the SAXS facility at the UQ Centre of Microscopy and Microanalysis, and the UQ ROCX Diffraction Facility. This work was supported in part by grants from NIH (to A.H.C.) and Wellcome Trust (to M.S.). B.K. is an Australian Research Council (ARC) Federation Fellow and a National Health and Medical Research Council (NHMRC) Honorary Research Fellow, and J.K.F. was an NHMRC CJ Martin Fellow.

Received: July 7, 2009
Revised: May 4, 2010
Accepted: June 1, 2010
Published: September 7, 2010

REFERENCES

Adams, A., Gottschling, D.E., Kaiser, C.A., and Stearns, T. (1997). Methods in yeast genetics (Cold Spring Harbor, NY: Cold Spring Harbor Laboratory Press).

Andrade, M.A., and Bork, P. (1995). HEAT repeats in the Huntington's disease protein. Nat. Genet. *11*, 115–116.

Bayliss, R., Littlewood, T., and Stewart, M. (2000). Structural basis for the interaction between FxFG nucleoporin repeats and importin-beta in nuclear trafficking. Cell *102*, 99–108.

Bhardwaj, A., and Cingolani, G. (2010). Conformational selection in the recognition of the snurportin importin beta binding domain by importin beta. Biochemistry *49*, 5042–5047.

Boeke, J.D., Trueheart, J., Natsoulis, G., and Fink, G.R. (1987). 5-Fluoroorotic acid as a selective agent in yeast molecular genetics. Methods Enzymol. *154*, 164–175.

Bublitz, M., Holland, C., Sabet, C., Reichelt, J., Cossart, P., Heinz, D.W., Bierne, H., and Schubert, W.D. (2008). Crystal structure and standardized geometric analysis of InlJ, a listerial virulence factor and leucine-rich repeat protein with a novel cysteine ladder. J. Mol. Biol. *378*, 87–96.

Cansizoglu, A.E., and Chook, Y.M. (2007). Conformational heterogeneity of karyopherin beta2 is segmental. Structure *15*, 1431–1441.

CCP4 (Collaborative Computational Project, Number 4). (1994). The CCP4 suite: Programs for protein crystallography. Acta Crystallogr. D Biol. Crystallogr. *50*, 760–763.

Cingolani, G., Bednenko, J., Gillespie, M.T., and Gerace, L. (2002). Molecular basis for the recognition of a nonclassical nuclear localization signal by importin beta. Mol. Cell *10*, 1345–1353.

Cingolani, G., Petosa, C., Weis, K., and Muller, C.W. (1999). Structure of importin-beta bound to the IBB domain of importin-alpha. Nature *399*, 221–229.

Cingolani, G., Lashuel, H.A., Gerace, L., and Muller, C.W. (2000). Nuclear import factors importin alpha and importin beta undergo mutually induced conformational changes upon association. FEBS Lett. *484*, 291–298.

Conti, E., Muller, C.W., and Stewart, M. (2006). Karyopherin flexibility in nucleocytoplasmic transport. Curr. Opin. Struct. Biol. *16*, 237–244.

Cook, A., Fernandez, E., Lindner, D., Ebert, J., Schlenstedt, G., and Conti, E. (2005). The structure of the nuclear export receptor Cse1 in its cytosolic state reveals a closed conformation incompatible with cargo binding. Mol. Cell *18*, 355–367.

Cowieson, N.P., Kobe, B., and Martin, J.L. (2008). United we stand: combining structural methods. Curr. Opin. Struct. Biol. *18*, 617–622.

Darden, T., York, D., and Pedersen, L. (1993). Particle mesh Ewald (PME): a N log(N) method for Ewald sums in large systems. J. Chem. Phys. *98*, 10089–10092.

Davis, I.W., Leaver-Fay, A., Chen, V.B., Block, J.N., Kapral, G.J., Wang, X., Murray, L.W., Arendall, W.B., 3rd, Snoeyink, J., Richardson, J.S., and Richardson, D.C. (2007). MolProbity: all-atom contacts and structure validation for proteins and nucleic acids. Nucleic Acids Res. *35*, W375–W383.

Dong, X., Biswas, A., and Chook, Y.M. (2009a). Structural basis for assembly and disassembly of the CRM1 nuclear export complex. Nat. Struct. Mol. Biol. *16*, 558–560.

Dong, X., Biswas, A., Suel, K.E., Jackson, L.K., Martinez, R., Gu, H., and Chook, Y.M. (2009b). Structural basis for leucine-rich nuclear export signal recognition by CRM1. Nature *458*, 1136–1141.

Emsley, P., and Cowtan, K. (2004). Coot: model-building tools for molecular graphics. Acta Crystallogr. D Biol. Crystallogr. *60*, 2126–2132.

Forwood, J.K., Lonhienne, T.G., Marfori, M., Robin, G., Meng, W., Guncar, G., Liu, S.M., Stewart, M., Carroll, B.J., and Kobe, B. (2008). Kap95p binding induces the switch loops of RanGDP to adopt the GTP-bound conformation: implications for nuclear import complex assembly dynamics. J. Mol. Biol. *383*, 772–782.

Fukuhara, N., Fernandez, E., Ebert, J., Conti, E., and Svergun, D. (2004). Conformational variability of nucleo-cytoplasmic transport factors. J. Biol. Chem. *279*, 2176–2181.

Groves, M.R., Hanlon, N., Turowski, P., Hemmings, B.A., and Barford, D. (1999). The structure of the protein phosphatase 2A PR65/A subunit reveals the conformation of its 15 tandemly repeated HEAT motifs. Cell *96*, 99–110.

Hess, B., Bekker, H., Berendsen, H.J.C., and Fraaije, J.G.E. (1997). LINCS: A linear constraint solver for molecular simulations. J. Comput. Chem. *18*, 1463–1472.

Hodel, A.E., Harreman, M.T., Pulliam, K.F., Harben, M.E., Holmes, J.S., Hodel, M.R., Berland, K.M., and Corbett, A.H. (2006). Nuclear localization signal receptor affinity correlates with in vivo localization in Saccharomyces cerevisiae. J. Biol. Chem. *281*, 23545–23556.

Iovine, M.K., and Wente, S.R. (1997). A nuclear export signal in Kap95p is required for both recycling the import factor and interaction with the nucleoporin GLFG repeat regions of Nup116p and Nup100p. J. Cell Biol. *137*, 797–811.

Jorgensen, W.L., Chandrasekhar, J., Madura, J.D., Impey, R.W., and Klein, M.L. (1983). Comparison of simple potential functions for simulating liquid water. J. Chem. Phys. *79*, 926–935.

Jorgensen, W.L., Maxwell, D., and Tirado-Rives, J. (1996). Development and testing of the OPLS all-atom force field on conformational energetics and properties of organic liquids. J. Am. Chem. Soc. *118*, 11225–11236.

Kobe, B., and Kajava, A.V. (2000). When protein folding is simplified to protein coiling: the continuum of solenoid protein structures. Trends Biochem. Sci. *25*, 509–515.

Kobe, B., Gleichmann, T., Horne, J., Jennings, I.G., Scotney, P.D., and Teh, T. (1999). Turn up the HEAT. Structure *7*, R91–R97.

Konarev, P.V., Volkov, V.V., Sokolova, A.V., Koch, M.H.J., and Svergun, D.I. (2003). PRIMUS: a Windows PC-based system for small-angle scattering data analysis. J. Appl. Crystallogr. *36*, 1277–1282.

Konarev, P.V., Petoukhov, M.V., Volkov, V.V., and Svergun, D.I. (2006). ATSAS 2.1, a program package for small-angle scattering data analysis. J. Appl. Crystallogr. *39*, 277–286.

Kozin, M.B., and Svergun, D.I. (2001). Automated matching of high- and low-resolution structural models. J. Appl. Crystallogr. *34*, 33–41.

Lange, A., Mills, R.E., Lange, C.J., Stewart, M., Devine, S.E., and Corbett, A.H. (2007). Classical nuclear localization signals: definition, function, and interaction with importin alpha. J. Biol. Chem. *282*, 5101–5105.

Lee, S.J., Imamoto, N., Sakai, H., Nakagawa, A., Kose, S., Koike, M., Yamamoto, M., Kumasaka, T., Yoneda, Y., and Tsukihara, T. (2000). The adoption of a twisted structure of importin-beta is essential for the protein-protein interaction required for nuclear transport. J. Mol. Biol. *302*, 251–264.

Lee, S.J., Sekimoto, T., Yamashita, E., Nagoshi, E., Nakagawa, A., Imamoto, N., Yoshimura, M., Sakai, H., Chong, K.T., Tsukihara, T., and Yoneda, Y. (2003). The structure of importin-beta bound to SREBP-2: nuclear import of a transcription factor. Science *302*, 1571–1575.

Lee, S.J., Matsuura, Y., Liu, S.M., and Stewart, M. (2005). Structural basis for nuclear import complex dissociation by RanGTP. Nature *435*, 693–696.

Lindahl, E., Hess, B., and van der Spoel, D. (2001). GROMACS 3.0: a package for molecular simulation and trajectory analysis. J. Mol. Model. *7*, 306–317.

Liu, S.M., and Stewart, M. (2005). Structural basis for the high-affinity binding of nucleoporin Nup1p to the Saccharomyces cerevisiae importin-beta homologue, Kap95p. J. Mol. Biol. *349*, 515–525.

Mitrousis, G., Olia, A.S., Walker-Kopp, N., and Cingolani, G. (2008). Molecular basis for the recognition of snurportin 1 by importin beta. J. Biol. Chem. *283*, 7877–7884.

Monecke, T., Guttler, T., Neumann, P., Dickmanns, A., Gorlich, D., and Ficner, R. (2009). Crystal structure of the nuclear export receptor CRM1 in complex with Snurportin1 and RanGTP. Science *324*, 1087–1091.

Murshudov, G.N., Vagin, A.A., and Dodson, E.J. (1997). Refinement of macromolecular structures by the maximum-likelihood method. Acta Crystallogr. D Biol. Crystallogr. *53*, 240–255.

Painter, J., and Merritt, E.A. (2006). Optimal description of a protein structure in terms of multiple groups undergoing TLS motion. Acta Crystallogr. D Biol. Crystallogr. *62*, 439–450.

Peifer, M., Berg, S., and Reynolds, A.B. (1994). A repeating amino acid motif shared by proteins with diverse cellular roles. Cell *76*, 789–791.

Petosa, C., Schoehn, G., Askjaer, P., Bauer, U., Moulin, M., Steuerwald, U., Soler-Lopez, M., Baudin, F., Mattaj, I.W., and Muller, C.W. (2004). Architecture of CRM1/Exportin1 suggests how cooperativity is achieved during formation of a nuclear export complex. Mol. Cell *16*, 761–775.

Qi, G., Lee, R., and Hayward, S. (2005). A comprehensive and non-redundant database of protein domain movements. Bioinformatics *21*, 2832–2838.

Roman, N., Kirkby, B., Marfori, M., Kobe, B., and Forwood, J.K. (2009). Crystallization of the flexible nuclear import receptor importin-beta in the unliganded state. Acta Crystallogr. Sect. F Struct. Biol. Cryst. Commun. *65*, 625–628.

Rubinstein, M., and Colby, R.H. (2004). Polymer physics (New York: Oxford University Press).

Sambrook, J., and Russel, D. (2001). Molecular cloning: A laboratory manual (Cold Spring Harbor: Cold Spring Harbor Laboratory Press).

Schlenstedt, G., Wong, D.H., Koepp, D.M., and Silver, P.A. (1995). Mutants in a yeast Ran binding protein are defective in nuclear transport. EMBO J. *14*, 5367–5378.

Shulga, N., Roberts, P., Gu, Z., Spitz, L., Tabb, M.M., Nomura, M., and Goldfarb, D.S. (1996). In vivo nuclear transport kinetics in Saccharomyces cerevisiae: a role for heat shock protein 70 during targeting and translocation. J. Cell Biol. *135*, 329–339.

Stewart, M. (2007). Molecular mechanism of the nuclear protein import cycle. Nat. Rev. Mol. Cell Biol. *8*, 195–208.

Storoni, L.C., McCoy, A.J., and Read, R.J. (2004). Likelihood-enhanced fast rotation functions. Acta Crystallogr. D Biol. Crystallogr. *60*, 432–438.

Suel, K.E., Cansizoglu, A.E., and Chook, Y.M. (2006). Atomic resolution structures in nuclear transport. Methods *39*, 342–355.

Svergun, D.I. (1992). Determination of the regularization parameter in indirect-transform methods using perceptual criteria. J. Appl. Crystallogr. *25*, 495–503.

Svergun, D.I. (1999). Restoring low resolution structure of biological macromolecules from solution scattering using simulated annealing. Biophys. J. *76*, 2879–2886.

Svergun, D.I., Barberato, C., and Koch, M.H. (1995). CRYSOL—a program to evaluate x-ray solution scattering of biological macromolecules from atomic coordinates. J. Appl. Crystallogr. *28*, 768–773.

Towbin, H., Staehelin, T., and Gordon, J. (1979). Electrophoretic transfer of proteins from polyacrylamide gels to nitrocellulose sheets: procedure and some applications. Proc. Natl. Acad. Sci. USA *76*, 4350–4354.

Vetter, I.R., Arndt, A., Kutay, U., Gorlich, D., and Wittinghofer, A. (1999). Structural view of Ran-importin beta interaction at 2.3 Å resolution. Cell *97*, 635–646.

Volkov, V.V., and Svergun, D.I. (2003). Uniqueness of ab initio shape determination in small-angle scattering. J. Appl. Crystallogr. *36*, 860–864.

Wohlwend, D., Strasser, A., Dickmanns, A., and Ficner, R. (2007). Structural basis for RanGTP independent entry of spliceosomal U snRNPs into the nucleus. J. Mol. Biol. *374*, 1129–1138.

Wright, P.E., and Dyson, H.J. (1999). Intrinsically unstructured proteins: re-assessing the protein structure-function paradigm. J. Mol. Biol. *293*, 321–331.

Zachariae, U., and Grubmuller, H. (2008). Importin-beta: structural and dynamic determinants of a molecular spring. Structure *16*, 906–915.

Zwart, P.H., Afonine, P.V., Grosse-Kunstleve, R.W., Hung, L.W., Ioerger, T.R., McCoy, A.J., McKee, E., Moriarty, N.W., Read, R.J., Sacchettini, J.C., et al. (2008). Automated structure solution with the PHENIX suite. Methods Mol. Biol. *426*, 419–435.